Advancements in Underwater Optical Wireless Communication: Channel Modeling, PAPR Reduction, and Simulations With OFDM

Liwei Yang, Zeyang Bi, Xue Liang, Lihao Zhao, Jiade Zhang, and Jingyi Peng

***Abstract*—Compared to underwater radio waves and acoustic communication technology, underwater optical communication technology has emerged as a technical means of underwater data and information transmission. Due to the complexity and volatility of the channel environment and the various factors that affect optical data transmission, there is no standard theoretical model for underwater optical wireless communication (UOWC). This work systematically evaluated and validated several optical attenuation models, leading to the development of an approach that significantly improves the accuracy of optical signal behavior prediction in underwater environments. The simulations using the Monte Carlo algorithm revealed critical insights into signal propagation, enabling more precise modeling of UOWC channels under varying conditions. We developed and validated a novel PTS-Clipping technique that effectively reduces PAPR by up to 15%, outperforming traditional methods and maintaining system efficiency. The novel PTS-Clipping approach achieved a reduction in OFDM signal PAPR from 11.861 dB to as low as 10.228 dB, demonstrating superior performance, particularly in high-order modulation schemes like 16-QAM, where signal integrity is critical. Theoretical analysis is combined with simulation experiments to promote a more robust and efficient UOWC system.**

***Index Terms*—OFDM, PAPR, underwater wireless optical communications.**

I. Introduction

With the increase in human underwater exploration activities and the rapid growth in the amount of data exchanged between devices, the need for underwater wireless communication technology has continued to grow. Compared to terrestrial and space links, underwater wireless communication links are more challenging. For atmospheric links, radio frequency (RF) waves are a good choice due to their high data rate, bandwidth, and speed. However, although RF waves can improve the data rate over short distances in underwater wireless communications, they attenuate significantly as the frequency increases, especially in seawater, where RF waves do not propagate well in good conductors such as salt water. Therefore, two types of communication technologies based on acoustic waves and wireless optical signals, have emerged in underwater wireless communication research. Underwater acoustic wave wireless communication (UAWC) [1], [2], [3] has the advantage of covering long distances. However, underwater acoustic wireless communication faces challenges such as narrow available bandwidth (limited to a few kbps), high propagation delay, strong signal attenuation, multipath propagation delay, and fast fading due to the Doppler effect [4]. For underwater optical wireless communication (UOWC) systems, there are advantages such as high data carrying capacity, high transmission rate, and low delay, which will support devices that require high-speed underwater wireless links, such as Unmanned underwater vehicles (UUV), sensors, autonomous underwater vehicles (AUV), submarines, and exploration ships [5], [6], [7], [8], [9]. UOWC also suffers from high attenuation due to water absorption and scattering effects caused by suspended particles, but this attenuation is smaller compared to RF attenuation over long distances. As shown in Fig. 1, to complete more complex and accurate underwater operations, the communication demand for such operations is increasing. Therefore, UOWC technology has attracted much attention in recent years [10], [11].

In the practical modeling of optical communication channels, the absorption and scattering effects on light propagating through seawater are some of the key influencing factors [12]. The absorption and scattering effects in seawater are mainly determined by its turbidity, particle type, and suspended matter [6], [10], [13]. In addition, absorption reduces the photon energy and limits the transmission distance. Scattering causes photons to diffuse in different directions, and the number of photons received is reduced due to the limited receiving aperture. Additionally, the scattering effect leads to differences in the time it takes for the photons to reach the receiving end, causing multipath delays.

When the UOWC system joins OFDM, some sub-carriers will inevitably stack during the Fast Fourier phase, leading to a high PAPR after the Fast Fourier transform (FFT) [14]. When the signal's peak value exceeds the linear working range of the

Received 24 August 2024; revised 30 September 2024; accepted 2 October 2024. Date of publication 9 October 2024; date of current version 16 October 2024. This work was supported in part by the National Natural Science Foundation of China under Grant 61705260 and in part by the 2115 Talent Development Program of China Agricultural University. *(Corresponding author: Liwei Yang.)*

Liwei Yang, Zeyang Bi, Xue Liang, and Jiade Zhang are with the College of Information and Electrical Engineering, China Agricultural University, Beijing 100083, China (e-mail: yangliwei@cau.edu.cn; bizeyang@cau.edu.cn; 3252625818@qq.com; 765743690@qq.com).

Lihao Zhao is with the College of Mechanical Electrical Engineering, Beijing Information and Technology University, Beijing 100192, China (e-mail: zlh_it@163.com).

Jingyi Peng is with China Industrial Control Systems Cyber Emergency Response Team, Beijing 100040, China (e-mail: dorispjy@163.com).

Digital Object Identifier 10.1109/JPHOT.2024.3475448

Fig. 1. Typical scenario of underwater wireless optical communication.

communication device, the communication performance will deteriorate. Therefore, it is critical to investigate strategies for reducing PAPR in the OFDM-based UOWC system. Previous studies have shown that a larger DC bias is usually required to eliminate clipping distortion, which reduces the energy efficiency of the system [15], [16]. According to [17], a smaller DC bias is used and a unipolar signal is obtained by clipping, but this reduces the reliability of the system. PAPR suppression algorithms for existing OFDM/OQAM systems are mainly based on the improvement of conventional OFDM algorithms. The PAPR suppression algorithms in OFDM systems are classified into distortion algorithms and non-distortion algorithms based on whether they cause distortion or not [18]. Distortion algorithms include clipping [19] and companding [20], etc., while non-distortion algorithms include selective mapping (SLM) [21], [22], partial transmission sequences (PTS) [23], [24], and tone reservation (TR) [25].

Among the above algorithms, the clipping method can be directly applied to OFDM systems, but it generates nonlinear distortion [18]. To solve these problems, in [26], the authors proposed a hybrid algorithm combining selective mapping (SLM), PTS, and companding techniques for PAPR reduction in Non-Orthogonal Multiple Access (NOMA) waveforms, highlighting the effectiveness of this approach with low computational complexity. In [27], the authors analyzed the performance of a two-piecewise linear companding technique for filtered-OFDM systems, focusing on PAPR and bit error rate (BER). In [28], the authors proposed a discrete elephant herding optimization-based partial transmit sequence (DEHO-PTS) scheme designed to minimize the PAPR of Universal Filtered Multi-Carrier (UFMC) signals. In [29], the authors introduced a hybrid precoded-companding scheme to reduce PAPR in NOMA systems. Different PAPR reduction methods are listed in Table I. However, excessive compression may cause signal distortion. Therefore, this paper proposes the PTS-Clipping algorithm to achieve PAPR reduction without significantly increasing the computational complexity. Compared to other complex PAPR reduction techniques, PTS-Clipping provides a better balance between performance and computational complexity.

The following are the main contributions of this paper:

1) This study provides an in-depth analysis of the optical transmission characteristics of seawater, incorporating various attenuation models to ascertain a comprehensive representation and mathematical model of the total attenuation coefficient and the multipath effects.
2) Comparing the performance of these algorithms when used with different numbers of subcarriers. It has been found that as the number of subcarriers increases, the PAPR of the system decreases. However, the computational complexity of the system increases as the number of subcarriers increases. Therefore, a trade-off between performance and computational complexity must be made when selecting the number of subcarriers.
3) The proposed system has been implemented on a test platform and experiments have been conducted to evaluate its performance in a real-world environment. The results of these experiments indicate that the proposed system can achieve good performance in terms of bit error rate and data rate. The results of a MATLAB simulation indicate that the original OFDM signal is reduced from 11.861 dB to 11.125 dB, 11.194 dB, 10.486 dB, and 10.228 dB when Complementary Cumulative Distribution Function (CCDF) is 10^{-3} after SLM, SLM-Clipping, PTS, and PTS-Clipping. This study confirmed that the PTS-Clipping technique in UOWC improves system performance in terms of BER, signal reliability, and overall data transmission efficiency.

II. Underwater Wireless Optical Communication Channel

A. Underwater Communications Channel Characterization

Water molecules and dissolved salts (KCl, NaCl, MgCl2, and Na2SO4) are the leading light absorbers in pure seawater [8]. Pure seawater is generally absorptive, except within the 400 nm-500 nm window, which corresponds to the blue-green region of the visible light spectrum [8]. Table II depicts pure seawater's absorption and scattering coefficient values (with the wavelengths listed). Scientists from several nations have evaluated these values, and they are generally accepted by the public.

Utilizing the absorption coefficient data of pure water spanning wavelengths from 340 nm to 670 nm, the generation of Fig. 2 was accomplished through MATLAB. As detailed in Table II, the absorption coefficient of pure water exhibits an increasing trend with longer light wavelengths. Specifically, it is observed that light, encompassing wavelengths in the range of 340 nm to 570 nm, demonstrates relatively consistent absorption

TABLE I
SUMMARY OF DIFFERENT PAPR REDUCTION METHODS

Methods	Advantages	Disadvantages
PTS-PAPR-OFDM[21], [22]	Effective PAPR reduction, which can be further reduced by optimizing the phase rotation factor	Channel state information and side information remain unknown
SLM-PAPR-OFMD[19], [20]	SLM does not directly modify the signal. Therefore, it does not introduce additional distortion and has less impact on signal quality.	Complex calculations and poor real-time.
SLM-Clipping-OFDM	Ability to achieve low BER while maintaining low PAPR	Increasing the complexity of the system.
PTS-SLM-companding-NOMA[26]	Significantly reduces PAPR while effectively enhancing the robustness of signal transmission.	High computational complexity and it is difficult to implement.
DEHO-PTS-UFMC[28]	Significant PAPR reduction, side lobe suppression, and low computational complexity	FBMC is challenging to implement and increases the computational load, and it is not compatible with OFDM.
Companding-NOMA[29]	Effectively reduce PAPR and implement simple	Excessive compression may cause signal distortion
PTS-Clipping-OFDM (IN THIS WORK)	**Reduces computational load and reduces PAPR more effectively.**	**Optical parameters are required to balance performance and distortion**

TABLE II
ABSORPTION COEFFICIENT AND SCATTERING COEFFICIENT OF PURE SEAWATER

Wavel ength /nm	absorption coefficient /m	Scattering coefficient /m	wavel ength/ nm	absorption coefficient /m	scattering coefficient /m
340	0.0325	0.0118	510	0.0382	0.0020
350	0.0204	0.0103	520	0.0474	0.0019
360	0.0156	0.0091	530	0.0505	0.0017
370	0.0114	0.0073	540	0.0441	0.0016
380	0.0100	0.0071	550	0.0654	0.0015
390	0.0088	0.0065	560	0.0715	0.0014
400	0.0070	0.0058	570	0.0804	0.0013
410	0.0056	0.0052	580	0.1060	0.0012
420	0.0054	0.0047	590	0.1487	0.0011
430	0.0064	0.0042	600	0.2417	0.0011
440	0.0083	0.0038	610	0.2876	0.0010
450	0.0110	0.0035	620	0.3074	0.0009
460	0.0122	0.0031	630	0.3184	0.0009
470	0.0130	0.0029	640	0.3382	0.0008
480	0.0157	0.0026	650	0.3594	0.0007
490	0.0158	0.0024	660	0.4212	0.0007
500	0.0242	0.0022	670	0.4346	0.0006

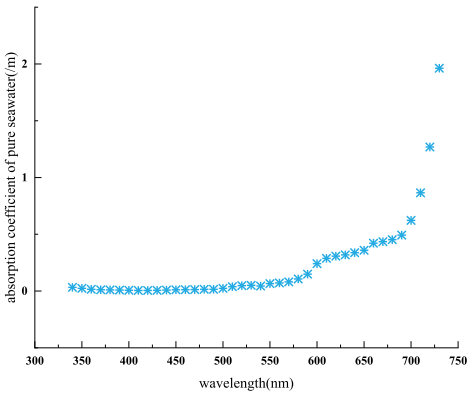

Fig. 2. Relationship between absorption coefficient and wavelength of pure seawater.

coefficients. However, a noteworthy increase in the absorption coefficient is observed within the range of 550 nm to 730 nm.

According to the formula (7) and the above values, Fig. 3 is obtained with MATLAB. As depicted in Fig. 3, the total absorption coefficient of seawater decreases with the increase of the wavelength of light at λ∈[340 nm,580 nm]. The absorption coefficient remains relatively constant in [500 nm, 600 nm]. The absorption coefficient of seawater smoothes out with increasing

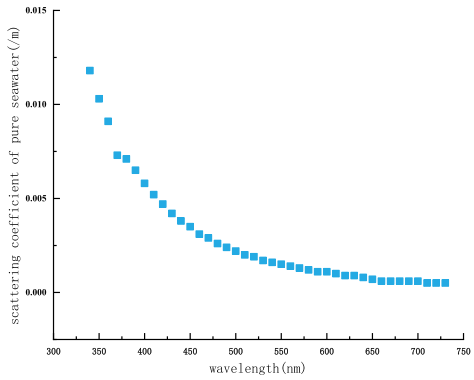

Fig. 3. Relationship between scattering coefficient and wavelength of pure seawater.

with λ∈[680 nm,730 nm]. These results demonstrate the absorption characteristics of light in pure seawater across different wavelengths. In the shorter wavelength range, seawater exhibits a stronger absorption of light, resulting in a higher absorption coefficient. As the wavelength increases, the absorption of light by pure seawater weakens, and the absorption coefficient gradually decreases. The absorption coefficient remains relatively stable within a specific range and does not vary with wavelength. However, in the more extended wavelength range, the absorption coefficient of seawater starts to increase again, albeit at a slower rate. These results are essential for designing and optimizing underwater optical communication.

Non-pigmented suspended particulates (NPSP) contain organic detritus from the decomposition of phytoplankton, suspended sediment, and sediment from the lake floor or resuspended from land. Light is both absorbed and scattered by non-pigmented suspended particles. The absorption coefficient and wavelength show an exponential decay. The formula for calculating the absorption coefficient is [30]:

$$a_l(\lambda) = a_l(\lambda_0)\exp[S(\lambda_0 - \lambda)] \quad (1)$$

In the formula (1), $a_l()$ is the light absorption coefficient of non-pigmented suspended particulates at the reference wavelength, generally taken as $=$ 400 nm [30]. And $a_l()$ equals 0.198 m^{-1} when is at 440 nm. S is the general slope of light

absorption. The absorption coefficients of non-pigmented suspended particles are obtained as follows:

$$\mathrm{a}_1(\lambda) = 0.198 \exp\left[0.01\,(440-\lambda)\right] \tag{2}$$

As illustrated from the formula (2), attenuates exponentially as the wavelength increases.

Phytoplankton is a type of tiny plant that lives in water. They are found on most of the planet's surface. Phytoplankton contributes to absorption predominantly via its body chlorophyll. According to the results of the literature survey, the average chlorophyll concentration is 5.5 mg/L. Phytoplankton has the following light absorption coefficient:

$$\mathrm{a}_f(\lambda) = \mathrm{a}_f^*(\lambda)\,[chl] \tag{3}$$

Where is the unit absorption coefficient of chlorophyll, [chl] is the chlorophyll concentration, and mg/m3 is the unit. The relationship between chlorophyll concentration and the unit absorption coefficient. The light absorption coefficient of phytoplankton is as follows:

$$\mathrm{a}_f(\lambda) = 0.06A(\lambda)\,5.5^{0.65} \tag{4}$$

In formula (4), A(λ) is the normalized unit absorption coefficient for the remaining wavelengths at 440 nm, with a value of 0.32. By combining the above formulas (3) and (4), we can get the wavelength of fixed light, and the absorption coefficient of phytoplankton will increase with the chlorophyll concentration. Dissolved organic matter in seawater gives the water a yellow color. Its spectral absorption coefficient can be derived from the following:

$$\mathrm{a}_h(\lambda) = \mathrm{a}_h(\lambda_0)\exp\left[S\,(\lambda_0-\lambda)\right] \tag{5}$$

In formula (5), the value of $a_h(\lambda_0)$ is 0.243 m^{-1}. The average slope of the absorption spectrum S is 0.014, and the absorption coefficient formula (6) is obtained by substituting the formula (5):

$$\mathrm{a}_h(\lambda) = 0.243 \exp\left[0.014\,(440-\lambda)\right] \tag{6}$$

The absorption of individual substances in seawater together determines the optical absorption properties of seawater. By combining the four subsections above, the total absorption coefficient of seawater can be derived [8], [30]:

$$a(\lambda) = a_s(\lambda) + a_l(\lambda) + a_h(\lambda) + a_f(\lambda) \tag{7}$$

In formula (7), $a_s(\lambda)$ is the absorption coefficient of pure seawater, $a_f(\lambda)$ is the absorption coefficient of phytoplankton, $a_h(\lambda)$ is the absorption coefficient of soluble organic matter, and $a_l(\lambda)$ is the absorption coefficient of non-pigment suspended particles.

Fig. 4 depicts the effects of various seawater attenuation coefficients on the optical power attenuation at the receiving end within seawater channels. The Monte Carlo method is employed to model and simulate the optical transmission process in seawater. This analysis leads to the conclusion that when light is transmitted underwater, the seawater channel's characteristics must be considered. At a consistent transmission distance, it is observed that the optical power at the receiving end is directly proportional to the absorption coefficient of seawater. Precisely, a higher absorption coefficient corresponds to a lower relative received power. Fig. 4 highlights this relationship, revealing that when the transmission distance is 6 meters, the relative received power is -3.909 dB for a seawater attenuation coefficient of 0.15 m^{-1}, and it decreases to -10.4 dB when the attenuation coefficient is 0.399 m^{-1}. Furthermore, it is evident that under the same seawater attenuation coefficient, the optical power at the receiving end diminishes with increased transmission distance. For instance, when the seawater attenuation coefficient is 0.15 m^{-1}, the relative received power shifts from -1.303 dB to -5.212 dB within the transmission distance range of 2 to 8 meters. Similarly, when the seawater attenuation coefficient is 0.399 m^{-1}, the relative received power transitions from -3.466 dB to -13.86 dB across the same transmission distance range of 2 to 8 meters.

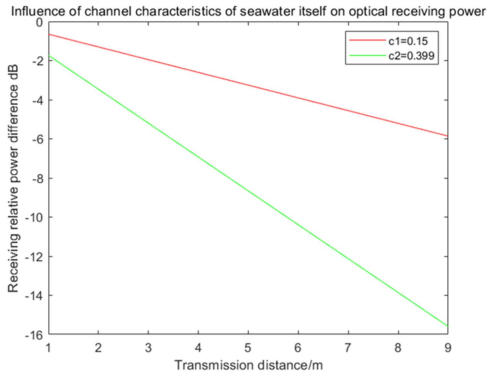

Fig. 4. The effect of seawater channel on the optical power attenuation at the receiving end in different seawater attenuation coefficients.

B. Absorption and Scattering

Light's passage through water primarily experiences attenuation due to absorption and scattering.

Generally, light propagation in water is governed by the wavelength-dependent total extinction coefficient, $c(\lambda)$. This coefficient quantifies the effects of absorption ($a(\lambda)$) and scattering ($b(\lambda)$) coefficients as in the formula [11], [31]:

$$c(\lambda) = \alpha(\lambda) + \beta(\lambda) \tag{8}$$

Here, α and β denote the contributions from absorption and scattering, while λ represents the transmission wavelength. Absorption refers to the medium's photon energy loss due to interactions with water molecules, dissolved substances, organic matter, phytoplankton, and particles. This process is influenced by changes in the medium's refractive index (n) and the light wavelength (λ). Scattering entails the light's deflection from its original path due to molecule or particle interactions. Water is categorized into types with nearly identical optical properties, based on their scattering and absorption characteristics.

C. Multipath Effect

Underwater, light wave propagation is impeded by absorption and scattering from the water column and suspended particles, and light waves are reflected and refracted when they encounter

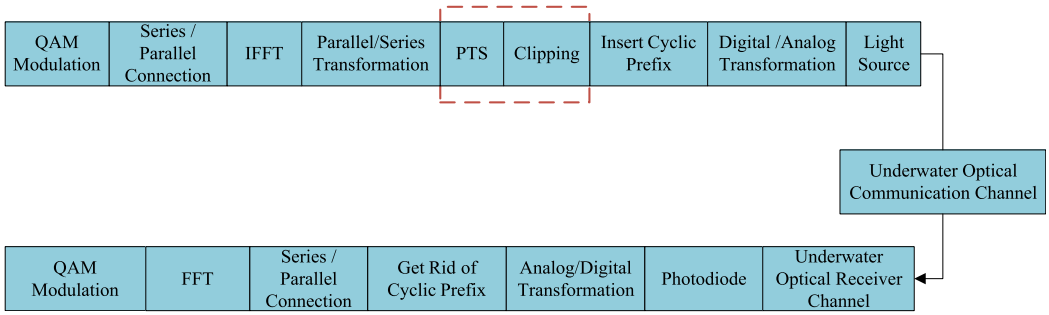

Fig. 5. The proposed OFDM block diagram for a UOWC system.

underwater obstacles such as rocks, marine organisms, or the water surface. This creates multiple propagation paths, resulting in the reception of duplicate signals, and time dilation from different signal arrival times on different paths increases inter-code interference (ISI). This is critical in high-speed data transmission, where ISI can severely disrupt signal demodulation and data recovery. Thus, multipath has a significant impact on the performance of UOWC.

The multipath effect model typically considers the propagation delay and attenuation of the signal on different paths. For each path, the signal experiences specific delay and gain variations.

$$x_{multipath}(t) = \sum_{i=1}^{n} x(t-\tau_i) \cdot g_i \tag{9}$$

In formula (9), $x(t)$ is the original signal, $x_{multipath}(t)$ is the signal processed by the multipath effect. τ_i is the first i path's delay. g_i is the first i path's gain vector.

III. PAPR Reduction With OFDM in UOWC

Orthogonal Frequency Division Multiplexing (OFDM) is a modulation technique commonly used in underwater communication due to its high data transmission rate, strong resistance to multipath interference, and high spectral efficiency [32], [33]. Fig. 5 shows the proposed OFDM block diagram for a UOWC system.

When the sample amplitude of a signal exceeds the threshold, the signal is clipped at this threshold with the phase unchanged. Linear operations such as PTS and SLM alter the phase of the transmitted signal to select the one with the lowest PAPR for transmission. While these methods maintain system performance and effectively reduce PAPR, they incur high computational complexity due to the need for multiple IFFT operations. In the proposed OFDM system illustrated in Fig. 5, a cyclic prefix (CP) is added to mitigate inter-symbol interference caused by multipath propagation. The length of the CP is determined based on the maximum delay spread of the channel, which is influenced by the number of channel taps. Specifically, the CP length is set to at least equal to the maximum delay spread to ensure effective mitigation of inter-symbol interference (ISI). Therefore, this paper proposes to combine PTS and SLM algorithms with the clipping technique to effectively reduce PAPR without significantly increasing the computational complexity. The PTS-Clipping method initially applies PTS to segment and adjust the OFDM signal, followed by clipping to further reduce PAPR. PTS processing steps divide firstly the OFDM signal X into V non-overlapping sub-blocks X_v, and secondly select a phase factor b_v for each sub-block X_v to minimize the composite signal's PAPR, and finally reassemble the phase-adjusted sub-blocks to form a new OFDM signal. Reducing PAPR is critical to maintaining signal quality in this context. However, clipping can introduce in-band and out-of-band noise, which can affect the bit error rate. To address this issue, a post-clipping filtering process is applied to mitigate noise effects. Specifically, after clipping, the signal is transformed into the frequency domain using an FFT, and high-frequency components outside the original bandwidth are removed. An inverse FFT (IFFT) then converts the filtered signal back to the time domain, smoothing in-band noise and mitigating its impact on BER performance. In iterative PTS-Clipping and SLM-Clipping techniques, this approach balances effective PAPR reduction with system performance without significantly increasing computational complexity.

Clipping processing steps apply clipping to the PTS-processed signal by setting a threshold A, limiting the amplitude of the signal:

$$x_{Clipped}(t) = \begin{cases} A \cdot e^{j\angle x(t)} & \text{if } |x(t)| > A \\ x(t) & \text{otherwise} \end{cases} \tag{10}$$

In formula (10), $x(t)$ represents the time-domain OFDM signal, A is the clipping threshold, and $\angle x(t)$ denotes the phase of $x(t)$.

When PTS is applied at the transmitter to reduce PAPR, it alters the phase of sub-blocks in the OFDM signal. To recover the original data phases at the receiver, side information that contains the phase rotation factors is transmitted alongside the OFDM signal. At the receiver, following the FFT conversion of the signal back to the frequency domain, these phase rotation factors are applied to reverse the PTS modifications and restore the original phases. Since the clipping process primarily affects the signal amplitude, it has minimal impact on phase recovery. Therefore, the receiver can accurately reconstruct the original signal phases before demodulation by utilizing side information.

Based on the above research and analysis, it is suggested that the pseudorandom sequences can be modulated using either Quadrature Amplitude Modulation (QAM) or Quadrature Phase Shift Keying (QPSK). In this context, QPSK is widely utilized in

various communication systems due to its lower implementation complexity and robust noise resistance [15]. However, QAM offers higher spectral efficiency and data transmission rates. Particularly under favorable channel conditions, QAM can more effectively utilize the available bandwidth, delivering higher bit rates. It is transformed into a low-speed parallel binary data stream. The OFDM signal is transformed into a time-domain signal using the Inverse Fast Fourier Transform (IFFT) and modulated in parallel with serial conversion, cyclic prefix insertion, and digital-to-analog conversion. The optical signal is sent via the underwater wireless channel, in which it conducts photoelectric conversion and inverse transformations to recover the original data.

Where n is the nth subcarrier x_n is the output signal obtained after IFFT:

$$x_n = \frac{1}{\sqrt{n}} X_k W_N^{nk} \tag{11}$$

Direct nonlinear operation is the principle of limiting amplitude at or near the peak of the OFDM signal to reduce PAPR [34]. First in the realization process is the mapping of frequency-domain signal x_{k} modulation. The realization process starts with the mapping and modulation of the frequency domain signal x_{k}. $\varphi(x_k)$ and $\theta(x_k)$ represents the different phase of x_{k}. Furthermore, the Fourier inverse transformation provides us with the signal in the time domain, x_{n}, which is derived from the limited frequency-domain signal $\tilde{\mathrm{x}}_{\mathrm{k}}$ after clipping. Suppose the OFDM system, after IFFT output signal is:

$$\tilde{x}_k = \begin{cases} x_k \cdot |x_k| \le A \\ A \cdot e^{j\theta(x_k)}, |x_k > A| \end{cases}, \varphi(x_k) = \text{angle}(x_k) \tag{12}$$

Orthogonal frequency division Multiplexing (OFDM) systems generate OFDM signals by modulating multiple subcarriers and combining the signals from each subcarrier. If the sub-carrier accumulation location is approximately at the peak point at a given moment, there will be a high peak power.

PAPR from the formula (13):

$$PAPR = \frac{P_{peak}}{P_{average}} = \frac{\max(|x_n|^2)}{E(|x_n|^2)} \tag{13}$$

IV. Simulation and Results

A. Simulation Parameters

In this paper, an OFDM signal processing framework designed for the UOWC system is mainly demonstrated by MATLAB software, and the simulation parameters are shown in Table III.

TABLE III
Simulation Parameters

Parameters	Value
Subcarrier number	256, 512, 1024
Oversampling factor	2, 4, 8
Photon number	106
Wavelength λ	0.924(um)
Half angle of divergence φ	0.419(°)
Waist radius/beam width w0	0.789(mm)
Number of SLM branches	4
PTS packet number	4
Clipping Limiting rate	4
Threshold A	2
Limiting threshold	6db
Attenuation factor	0.5
Multipath number	4
Water wavelengths	[340,730]
Cyclic Prefix Length	4
Iterations number	10 000

B. Simulation Result

Fig. 6 depicts the PAPR comparison of subcarriers n = 256, 512, and 1024. As shown in the graph, the PAPR increases with the number of subcarriers. As the number of sub-carriers increases, the probability of experiencing the same sub-carrier phase increases, hence the PAPR increase.

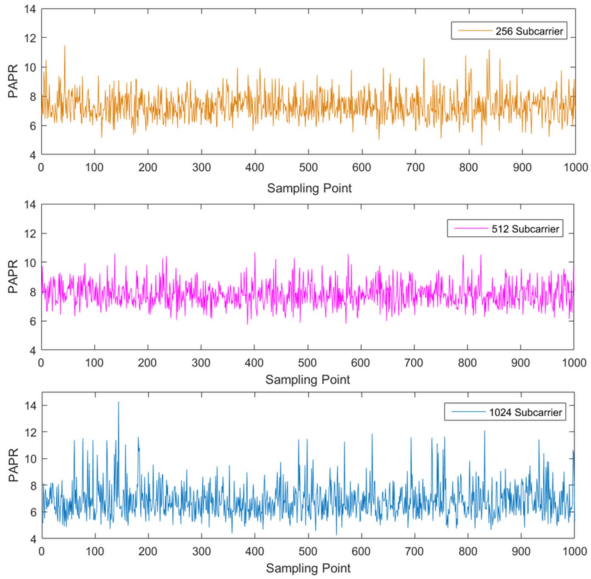

Fig. 6. Amplitude average of OFDM signal under different subcarriers.

Fig. 7 shows the typical effects that a wireless signal may encounter during underwater propagation: multipath effects and signal attenuation. The first row (Original Signal) displays the original transmitted signal as a clean sine wave. The second row (Signal after Multipath Effects) shows how the signal waveform is altered by multipath propagation, where the signal experiences multiple reflections and delays, resulting primarily in amplitude changes. The third row (Signal after Signal Attenuation) shows the signal after attenuation, simulating the energy loss due to absorption and scattering in the underwater environment, which further reduces the signal amplitude. It is important to note that while the multipath effects shown focus on amplitude changes, they do not reflect potential phase distortions which are also characteristic of multipath channels.

Fig. 8 represents the performance analysis of the reduction techniques for evaluating the PAPR, including Original, SLM,

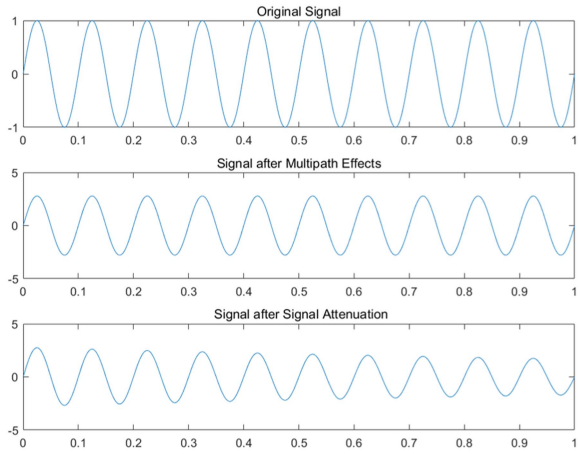

Fig. 7. Signal comparison after multipath effect and signal attenuation.

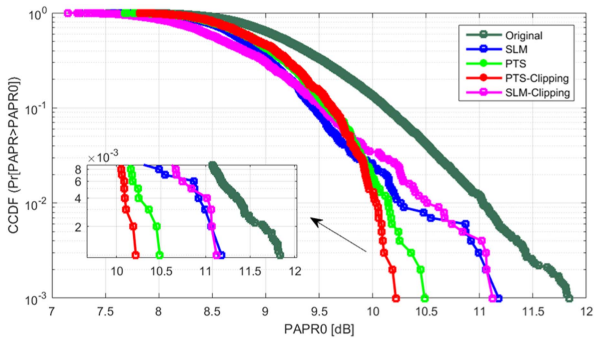

Fig. 8. The performance analysis of the reduction techniques for evaluating the PAPR.

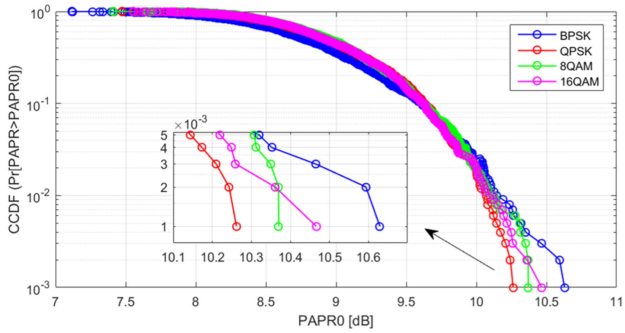

Fig. 9. The performance of the CCDF for different modulation techniques.

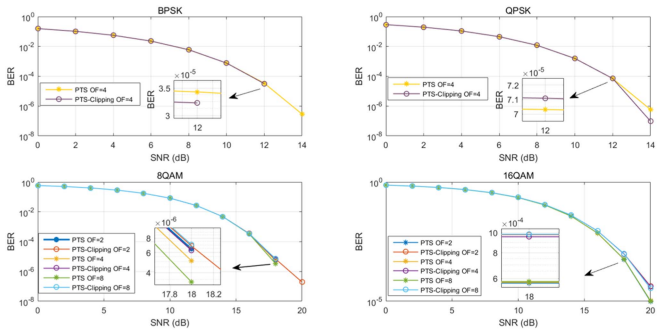

Fig. 10. The comparative performance of PTS and PTS-Clipping techniques over different modulation and oversampling factor schemes.

PTS, SLM-Clipping, and PTS-Clipping techniques. The X-axis represents the PAPR, Y-axis represents the CCDF, it can be seen from the figure that the Original curve has the highest probability at high PAPR values, and the application of SLM and PTS techniques significantly reduces the probability of high PAPR values, which indicates that these techniques are effective in reducing the peak power of the signal. When the SLM and PTS techniques are combined with clipping, the probability of occurrence of high PAPR values further decreases, indicating that clipping further enhances the effectiveness of SLM and PTS. The vignette zooms in on the CCDF curves for PAPR values in the 10 to 12 dB range, which reveal that the original OFDM signal is reduced from 11.861 dB to 11.125 dB, 11.194 dB, 10.486 dB, and 10.228 dB when CCDF is 10^{-3} after SLM, SLM-Clipping, PTS, and PTS-Clipping. Simulation results confirm that combining clipping with PTS and SLM effectively reduces PAPR without compromising BER performance.

Fig. 9 This image shows the performance of the CCDF for different modulation techniques in terms of peak-to-average power ratio (PAPR). These modulation techniques include Binary Phase Shift Keying (BPSK), Quadrature Phase Shift Keying (QPSK), 8-QAM, and 16-QAM. The X-axis denotes the PAPR, the Y-axis denotes the CCDF, and the curves represent the performance of the different modulation techniques on the PAPR. From the graph, we observe a higher probability of higher-order modulation techniques (e.g., 16-QAM) at high PAPR values compared to lower-order modulation (e.g., BPSK and QPSK). The small window chart zooms in on the portion of the PAPR values between 10.1 and 10.6 dB to show more clearly the performance differences between the different modulation techniques. A sharp increase in the CCDF value for 16-QAM is observed in this interval, indicating a rapid increase in the probability of higher-order modulated signals at this PAPR level.

Fig. 10 illustrates the BER performance for BPSK, QPSK, 8-QAM, and 16-QAM under PTS and PTS-Clipping techniques with varying oversampling factors (OFs). Each subplot shows the variation in BER as the SNR increases. In the BPSK plot (top left), at SNR = 12 dB, the PTS-Clipping curve falls below the PTS curve, indicating improved BER. For QPSK (top right), PTS-Clipping slightly underperforms compared to PTS at 12 dB but shows improvement at higher SNRs. For 8-QAM (bottom left), at an SNR of 18 dB, BER improves with increasing oversampling factors (OFs) without clipping. When the SNR exceeds 18 dB, only PTS-Clipping with an oversampling factor of 2 retains its performance. For 16-QAM (bottom right), at 18 dB, the lowest BER is achieved with PTS at lower OFs. However, at an SNR of 20 dB, PTS-Clipping with an oversampling factor of 8 achieves the lowest BER, followed by OFs of 4 and 2. This suggests that clipping becomes more effective at higher SNRs, especially when higher OFs are used. In conclusion, PTS-Clipping generally improves BER at higher SNRs, particularly for higher-order modulations. Its effectiveness depends on the modulation scheme and the OF.

V. Conclusion

This paper thoroughly explores the complex challenges in UOWC, with a focus on channel modeling and signal quality enhancement through advanced PAPR reduction techniques. Initially, the study examines the optical properties of seawater in detail, developing a robust model that accounts for both the total attenuation coefficient and the complex multipath effects common in underwater environments. This model lays the groundwork for further research and development in UOWC systems. Furthermore, we introduce and rigorously evaluate a novel PAPR reduction technique, the PTS-Clipping method, which synergistically combines the benefits of partial transmission sequence and clipping approaches. Our findings indicate that this method significantly reduces PAPR while maintaining lower computational complexity compared to traditional techniques. This improvement proves particularly effective in high-order modulation schemes critical for maintaining signal integrity. In conclusion, the advancements detailed in this paper enhance the development of efficient and reliable UOWC systems, promoting new modulation techniques to address the challenging conditions of underwater communication.

References

[1] M. Stojanovic and J. Preisig, "Underwater acoustic communication channels: Propagation models and statistical characterization," *IEEE Commun. Mag.*, vol. 47, no. 1, pp. 84–89, Jan. 2009, doi: 10.1109/mcom.2009.4752682.

[2] P. A. Van Walree, "Propagation and scattering effects in underwater acoustic communication channels," *IEEE J. Ocean. Eng.*, vol. 38, no. 4, pp. 614–631, Oct. 2013, doi: 10.1109/joe.2013.2278913.

[3] D. Pompili, T. Melodia, and I. F. Akyildiz, "A CDMA-based medium access control for underwater acoustic sensor networks," *IEEE Trans. Wireless Commun.*, vol. 8, no. 4, pp. 1899–1909, Apr. 2009, doi: 10.1109/twc.2009.080195.

[4] M. Sasano et al., "Development of a regional underwater positioning and communication system for control of multiple autonomous underwater vehicles," in *Proc. 2016 IEEE/OES Auton. Underwater Veh.*, Tokyo, Japan, Nov. 2016, pp. 431–434, doi: 10.1109/AUV.2016.7778708.

[5] J. Wang, C. Lu, S. Li, and Z. Xu, "100 m/500 mbps underwater optical wireless communication using an NRZ-OOK modulated 520 nm laser diode," *Opt. Exp.*, vol. 27, no. 9, Apr. 2019, Art. no. 12171, doi: 10.1364/oe.27.012171.

[6] M. F. Ali, D. N. K. Jayakody, and Y. Li, "Recent trends in underwater visible light communication (UVLC) systems," *IEEE Access*, vol. 10, pp. 22169–22225, 2022, doi: 10.1109/ACCESS.2022.3150093.

[7] S. Zhu, X. Chen, X. Liu, G. Zhang, and P. Tian, "Recent progress in and perspectives of underwater wireless optical communication," *Prog. Quantum Electron.*, vol. 73, Sep. 2020, Art. no. 100274, doi: 10.1016/j.pquantelec.2020.100274.

[8] Z. Zeng, S. Fu, H. Zhang, Y. Dong, and J. Cheng, "A survey of underwater optical wireless communications," *IEEE Commun. Surveys Tut.*, vol. 19, no. 1, pp. 204–238, Firstquarter 2017, doi: 10.1109/comst.2016.2618841.

[9] M. F. Ali, D. N. K. Jayakody, Y. A. Chursin, S. Affes, and S. Dmitry, "Recent advances and future directions on underwater wireless communications," *Arch. Comput. Methods Eng.*, vol. 27, no. 5, pp. 1379–1412, Nov. 2020, doi: 10.1007/s11831-019-09354-8.

[10] C. Zou, F. Yang, J. Song, and Z. Han, "Underwater wireless optical communication with one-bit quantization: A hybrid autoencoder and generative adversarial network approach," *IEEE Trans. Wireless Commun.*, vol. 22, no. 10, pp. 6432–6444, Oct. 2023, doi: 10.1109/TWC.2023.3243212.

[11] G. Schirripa Spagnolo, L. Cozzella, and F. Leccese, "Underwater optical wireless communications: Overview," *Sensors*, vol. 20, no. 8, Apr. 2020, Art. no. 2261, doi: 10.3390/s20082261.

[12] Z. Lin, G. Xu, Q. Zhang, and Z. Song, "Average symbol error probability and channel capacity of the underwater wireless optical communication systems over oceanic turbulence with pointing error impairments," *Opt Exp.*, vol. 30, no. 9, Apr. 2022, Art. no. 15327, doi: 10.1364/OE.457043.

[13] C. Zou, F. Yang, J. Song, and Z. Han, "Underwater optical channel generator: A generative adversarial network based approach," *IEEE Trans. Wireless Commun.*, vol. 21, no. 11, pp. 9394–9403, Nov. 2022, doi: 10.1109/TWC.2022.3176208.

[14] S. Chi, P. Wang, S. Niu, H. Che, Z. Wang, and Y. Wu, "Uniformity improvement on received optical power for an indoor visible light communication system with an angle diversity receiver," *Appl. Opt.*, vol. 60, no. 26, pp. 8031–8037, 2021, doi: 10.1364/ao.432653.

[15] J. Wang, Y. Guo, and X. Zhou, "PTS-clipping method to reduce the PAPR in ROF-OFDM system," *IEEE Trans. Consum. Electron.*, vol. 55, no. 2, pp. 356–359, May 2009, doi: 10.1109/tce.2009.5174393.

[16] J. B. Carruthers and J. M. Kahn, "Multiple-subcarrier modulation for nondirected wireless infrared communication," *IEEE J. Sel. Areas Commun.*, vol. 14, no. 3, pp. 538–546, Apr. 1996, doi: 10.1109/49.490239.

[17] J. Armstrong and B. J. C. Schmidt, "Comparison of asymmetrically clipped optical OFDM and DC-biased optical OFDM in AWGN," *IEEE Commun. Lett.*, vol. 12, no. 5, pp. 343–345, May 2008, doi: 10.1109/lcomm.2008.080193.

[18] Y. Li, H. Qiu, X. Chen, and J. Fu, "A novel PAPR reduction algorithm for DCO-OFDM/OQAM system in underwater VLC," *Opt. Commun.*, vol. 463, May 2020, Art. no. 125449, doi: 10.1016/j.optcom.2020.125449.

[19] J. Armstrong, "New OFDM peak-to-average power reduction scheme," in *Proc. IEEE VTS 53rd Veh. Technol. Conf., Spring*, Rhodes, Greece, 2001, vol. 1, pp. 756–760, doi: 10.1109/vetecs.2001.944945.

[20] X. Wang, T. T. Tjhung, and C. S. Ng, "Reduction of peak-to-average power ratio of OFDM system using a companding technique," *IEEE Trans. Broadcast.*, vol. 45, no. 3, pp. 303–307, Sep. 1999, doi: 10.1109/11.796272.

[21] S.-Y. Zhang and B. Shahrrava, "A SLM scheme for PAPR reduction in polar coded OFDM-IM systems without using side information," *IEEE Trans. Broadcast.*, vol. 67, no. 2, pp. 463–472, Jun. 2021, doi: 10.1109/TBC.2020.3039696.

[22] J. Ji and G. Ren, "A new modified SLM scheme for wireless OFDM systems without side information," *IEEE Signal Process. Lett.*, vol. 20, no. 11, pp. 1090–1093, Nov. 2013, doi: 10.1109/lsp.2013.2278286.

[23] D.-W. Lim, S.-J. Heo, J.-S. No, and H. Chung, "A new PTS OFDM scheme with low complexity for PAPR reduction," *IEEE Trans. Broadcast.*, vol. 52, no. 1, pp. 77–82, Mar. 2006, doi: 10.1109/tbc.2005.861605.

[24] S.-J. Ku, C.-L. Wang, and C.-H. Chen, "A reduced-complexity PTS-based PAPR reduction scheme for OFDM systems," *IEEE Trans. Wireless Commun.*, vol. 9, no. 8, pp. 2455–2460, Aug. 2010, doi: 10.1109/twc.2010.062310.100191.

[25] B. Wang, Q. Si, and M. Jin, "A novel tone reservation scheme based on deep learning for PAPR reduction in OFDM systems," *IEEE Commun. Lett.*, vol. 24, no. 6, pp. 1271–1274, Jun. 2020, doi: 10.1109/LCOMM.2020.2980832.

[26] A. Kumar, N. Gour, H. Sharma, and R. Pareek, "A hybrid technique for the PAPR reduction of NOMA waveform," *Int. J. Commun. Syst.*, vol. 36, no. 4, Mar. 2023, Art. no. e5412, doi: 10/gt7sm4.

[27] M. Al-Gharabally, A. F. Almutairi, and A. Krishna, "Performance analysis of the two-piecewise linear companding technique on filtered-OFDM systems," *IEEE Access*, vol. 9, pp. 48793–48802, 2021, doi: 10.1109/ACCESS.2021.3068371.

[28] Ş. Şimşir and N. Taşpınar, "A novel discrete elephant herding optimization-based PTS scheme to reduce the PAPR of universal filtered multicarrier signal," *Eng. Sci. Technol., an Int. J.*, vol. 24, no. 6, pp. 1428–1441, Dec. 2021, doi: 10.1016/j.jestch.2021.03.001.

[29] A. Kumar, N. Gour, and H. Sharma, "A CA and ML approach for M-MIMO optical non-orthogonal multiple access power efficiency," *J. Opt. Commun.*, Sep. 2023, doi: 10.1515/joc-2023-0194.

[30] N. G. Jerlov, *Marine Optics*. New York, NY, USA: Elsevier, 1976.

[31] M. Darwiesh, A. F. El-Sherif, H. S. Ayoub, Y. H. El-sharkawy, M. F. Hassan, and Y. H. Elbashar, "Hyperspectral laser imaging of underwater targets," *J. Opt.-UK*, vol. 47, no. 4, pp. 553–560, Dec. 2018, doi: 10/gt7sxc.

[32] J. Chen, L. Zhao, M. Jiang, and Z. Wu, "Sherman-morrison formula aided adaptive channel estimation for underwater visible light communication with fractionally-sampled OFDM," *IEEE Trans. Signal Process.*, vol. 68, pp. 2784–2798, 2020, doi: 10.1109/TSP.2020.2988355.

[33] T. Essalih, M. A. Khalighi, S. Hranilovic, and H. Akhouayri, "Optical OFDM for SiPM-based underwater optical wireless communication links," *Sensors*, vol. 20, no. 21, Oct. 2020, Art. no. 6057, doi: 10.3390/s20216057.

[34] Y. Ding, L. Xue, and Z. Wang, "A novel precoding technique to reduce PAPR of UCA-OAM systems," *IEEE Commun. Lett.*, vol. 26, no. 8, pp. 1903–1907, Aug. 2022, doi: 10.1109/lcomm.2022.3175991.